Available online at www.sciencedirect.com
ScienceDirect
Journal of Power Sources 168 (2007) 484–492
JOURNAL OF POWER SOURCES
www.elsevier.com/locate/jpowsour

Electrode structure analysis and surface characterization for lithium-ion cells simulated low-Earth-orbit satellite operation II: Electrode surface characterization

Xianming Wang [a,*], Toshiya Hironaka [b], Eiji Hayashi [b], Chisa Yamada [a], Hitoshi Naito [a], Go Segami [a], Yoko Sakiyama [b], Yoshikazu Takahashi [b], Koichi Kibe [a]

[a] *Institute of Space Technology and Aeronautics, Japan Aerospace Exploration Agency, Tsukuba Space Center, Sengen 2-1-1, Ibaraki 305-8505, Japan*
[b] *Toray Research Center, Inc., Sonoyama 3-3-7, Otsu, Shiga 520-8567, Japan*

Received 15 October 2006; received in revised form 30 January 2007; accepted 26 February 2007
Available online 12 March 2007

Abstract

As a sequence work to investigate the performance-degradation mechanism of an aged commercial laminated lithium-ion cell experiencing 4350-cycle charge–discharge in a simulated low-Earth-orbit (LEO) satellite operation, we performed the surface characterization of $LiCoO_2$ cathode and graphite anode by Fourier transform infrared-Attenuated total reflection (FTIR-ATR) and X-ray photoelectron spectroscopy (XPS) analysis in this work. Overall, the graphite anode had a larger change in surface chemistry than that of the $LiCoO_2$ cathode. Except the common surface components, we detected Co metal at the aged graphite surface in the first time. This Co metal deposition was believed to originate from Co^{2+} dissolution from $LiCoO_2$ cathode during prolonged cycling, and detrimental to structure stability of $LiCoO_2$ cathode which was a main cause of cell capacity loss. The amount of surface-film component was also estimated by FTIR analysis. Though the total amount of surface film increased, the organic (inorganic) surface film decreased (increased) with prolonged cycling.

Keywords: Lithium-ion cell; Satellite application; Surface characterization; Performance-degradation mechanism

1. Introduction

So far, it has been widely accepted that the charge–discharge behavior of a lithium-ion cell depends strongly on the nature of the passivation films developed on the graphite anode. Considerable effort was devoted to characterize the surface components of the graphite anode in the carbonate-based electrolytes. Some inorganic and organic compounds, such as lithium carbonate (Li_2CO_3), lithium oxide (Li_2O), lithium hydride (LiOH), lithium fluoride (LiF), lithium alkoxide (ROLi), lithium alkyl carbonate (ROCOOLi), and lithium alkyl carboxylate (RCOOLi), were detected by Fourier transform infrared spectroscopy (FTIR), X-ray photoelectron spectroscopy (XPS), scanning electron microscopy (SEM), and the other solid-surface analysis methods [1–17]. These surface components, also detected at lithium-metal surface immersed in a carbonate-based electrolyte, were disclosed to effectively prevent further reduction decomposition of solvents and solute on the graphite anode following a well-known solid electrolyte interphase (SEI) mechanism [18–20]. A few schematic illustrations were also proposed to demonstrate the surface film composition and morphology of graphite anode. Recently, similar SEI film was also observed on lithium transition metal oxide cathodes by some authors [21–25]. However, the previous attention was only paid to those lithium-ion systems for commercial purposes, which generally experiences short-term charge–discharge cycles. For long-term space applications, the lithium-ion cells operate in the special charge–discharge conditions, such as low taper voltage below 4.1 V, low charge and discharge rates of smaller than 1.0 C, consecutive charge–discharge cycles in low-Earth-orbit (LEO) missions, constant ambient temperature in an optimum value between 10 and 20 °C, and long cycle-life requirement (5 years for LEO, 15 years for geosynchronous-Earth-orbit (GEO)) [26,27]. One can expect that the electrode

* Corresponding author. Tel.: +81 29 868 4247; fax: +81 29 868 5969.
E-mail address: wangdai-666@mpd.biglobe.ne.jp (X. Wang).

0378-7753/$ – see front matter © 2007 Elsevier B.V. All rights reserved.
doi:10.1016/j.jpowsour.2007.02.081

surface chemistry of lithium-ion cells as power-storage devices of spacecraft is significantly different from those characterized so far. Therefore, it becomes essential to characterize the surface chemistry of graphite anode and lithium transition metal oxide cathode operated in a long-term charge–discharge cycle.

In order to understand the performance-degradation mechanism of these cells, we performed destructive physical analysis for an aged commercial laminated lithium-ion cell experiencing 4350-cycle charge–discharge in a simulated LEO satellite operation in paper I [28]. The electrochemical performance of graphite anode and $LiCoO_2$ cathode obtained from this aged cell was investigated by capacity verification, and the electrode's structure was explored by X-ray diffraction (XRD) and ^7Li nuclear magnetic resonance (NMR). The experimental results indicate that the $LiCoO_2$ cathode, rather than graphite anode, is responsible for the performance degradation of the aged lithium-ion cell. XRD analysis disclosed that the aged cathode exhibited a much larger structure change than the aged anode, and detected a new component with a large lattice constant in c axis in the aged cathode. NMR and XRD analysis of graphite anode detected the lithium ions that were irreversibly reserved inside graphite layer. Consequently, the lithium-ion deficiency (excess) occurred in the $LiCoO_2$ (graphite) structure, resulting in lattice constant increase in c-axis direction. We believe that the serious structure change in $LiCoO_2$ cathode was primarily responsible for the performance degradation of the aged lithium-ion cell experiencing long-term cycle-life testing.

In order to understand the myriad phenomena existing in a lithium-ion system, the concurrence of several analytic techniques is required. The present work aims at a comparative investigation on the surface layer of the graphite anodes and $LiCoO_2$ cathodes obtained from the aged and fresh laminated lithium-ion cells as mentioned in paper I [28]. Fourier transform infrared-attenuated total reflection (FTIR-ATR) analysis was used to characterize the organic components on the electrode surface. The inorganic components on the electrode surface were analyzed by XPS analysis. The correlation of electrode surface chemistry to cycling performance was also discussed.

2. Experimental

2.1. Sample preparation

One aged cell and one fresh cell were destructed under a highly pure argon atmosphere in a standard glove box (Miwa), as described in paper I [28]. The graphite anode and $LiCoO_2$ cathode materials were transported to instruments using airtight transfer vessels with a high-purity argon for surface characterization (FTIR-ATR and XPS). We did not wash the electrode surface before used for structure analysis and surface characterization since the surface film may partly dissolve in the washing solvent in our experience. In addition, the electrolyte salt peaks and EC contribution can be easily identified in the resulting spectra, which are useful to examine the ratio of the electrolyte decomposition components to the original surface film components.

The ambient temperature for the surface characterization was $22 \pm 3\,^{\circ}C$.

2.2. FTIR-ATR spectroscopy

The FTIR measurements were performed on a FTIR spectrometer (Bio Rad Digilab, FTS-60A/896) equipped with a broadband mercury–cadmium–telluride (MCT) detector under a high-purity argon atmosphere. The spectra were acquired in the attenuated total reflection (ATR) mode using a hemispherical Ge optic at a spectral resolution of $4\,cm^{-1}$ and averaged over 128 scans. All spectra were obtained from a 2.0 mm diameter area on samples pressed against the Ge crystal. The angle of incidence was fixed at 40° in this work, corresponding to the penetration depth of 0.76 μm.

2.3. XPS measurements

XPS measurements were carried out with a spectrometer (SSI, SSX-100) using a focused monochromatized Al Kα radiation. The analyzed area of the samples was an elliptic sharp of 1000 μm × 1750 μm for surface analysis or 300 μm × 525 μm for depth profiling. The take-off angle between the sample and analyzer entrance was set at 35° in order to enhance the surface sensitivity. Depth profiling was made by Ar ion-beam sputtering (3 keV). The sputtering time is estimated to be 3.7–4.0 nm min^{-1} for a SiO_2/Si film. The pressure in the analysis chamber was kept below 1×10^{-9} Torr.

Peaks assignments were made with respect to reference compounds, such as $LiPF_6$, LiF, Li_2CO_3, and $CH_3OCOOLi$, which could be present on the electrode surfaces. The binding energy scale was calibrated from the hydrocarbon using the C 1s peak at 284.6 eV.

3. Results and discussion

3.1. FTIR-ATR spectroscopy

FTIR is a powerful tool to acquire the organic information on a solid surface, and hence most commonly used to investigate the surface chemistry of the anode and cathode for a lithium-ion cell. The previous studies revealed that both $LiPF_6$ solute and alkyl carbonate solvent experienced redox decomposition with charge–discharge cycle and contributed to the buildup of the surface films by depositing the insoluble decomposition products. The analysis of the FTIR spectra measured from the anode and cathode in the present work is based on the previous studies [8–13].

Fig. 1(a and b) compares the FTIR spectra of surface films for $LiCoO_2$ cathode and graphite anode obtained from aged and fresh lithium-ion cells. Peak assignments are also present in these figures.

In Fig. 1(a), all two spectra have typical ROCOOLi peaks around $1072\,cm^{-1}$, and Li_2CO_3 peak around $875\,cm^{-1}$. The source of ROCOOLi and Li_2CO_3 detected on the cathode's surface by the FTIR measurement is not yet clear. Aurbach et al. believed that these species are formed on the anode side.

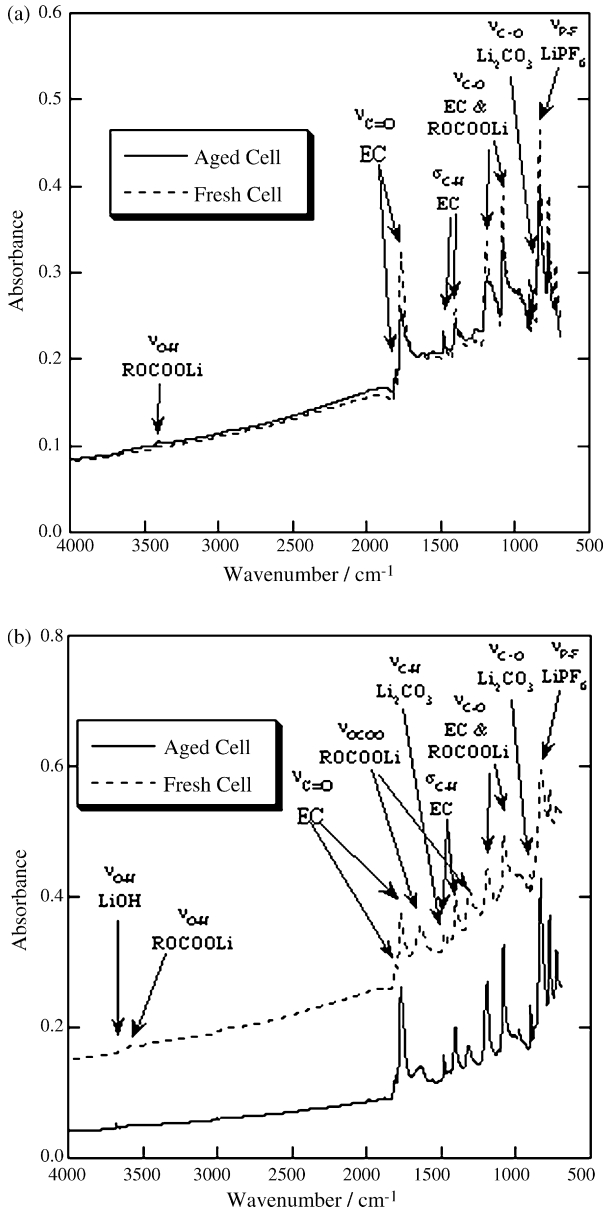

Fig. 1. FTIR spectra of surface films for (a) $LiCoO_2$ cathode and (b) graphite anode obtained from aged and fresh lithium-ion cells.

The electrolyte becomes saturated with these species after some cycling, and thus these species precipitate on the cathode's surface [24]. The peaks of EC solvent (1806, 1770, 1482, 1405, 1193, and 1085 cm^{-1}) and $LiPF_6$ solute (838 cm^{-1}) were also detected since the electrode surface kept an unwashed state. The EC peaks ranging from 1500 to 1000 cm^{-1} are probably superimposed with the peaks of ROCOOLi surface species which appear in the same wavenumber range.

The FTIR spectra in Fig. 1(b) exhibit more surface species on graphite anodes than those on $LiCoO_2$ cathode. Around 3680 cm^{-1}, a lithium hydride (LiOH) peak emerges in the FTIR spectra of the aged graphite anode surface. Since no corresponding peak may be observed for the graphite anode obtained from the fresh lithium-ion cell, we can reasonably attribute this LiOH peak to the electrolyte reduction decomposition on graphite anode due to prolonged cycling. Aurbach et al. argued that LiOH could not prevent the decomposition of electrolytes on graphite anode surface [29,30]. Additionally, we detected ROCOOLi (3587, 1640, 1320, and 1079 cm^{-1}), Li_2CO_3 (1485, 875–906 cm^{-1}), EC (1806, 1770, 1482, 1405, 1195, and 1086 cm^{-1}), and $LiPF_6$ (837 cm^{-1}).

Table 1
Peak intensity ratio of surface species to EC (1770 cm^{-1}) on aged and fresh graphite anodes obtained from Fig. 1(b)

Graphite anode	ROCOOLi	LiOH
	1640 cm^{-1}	3680 cm^{-1}
Aged	0.18	0.05
Fresh	0.64	0

As described in experimental section, we did not wash the sample electrodes prior to FTIR analysis. Since EC is a solid at room temperature and nonvolatile, we can use EC peak around 1770 cm^{-1} as a standard intensity to compare the peak intensities of the other surface components. Generally, the decomposed EC amount is enough small compared to the total EC content in the bulk electrolyte. Therefore, it is reasonable to assume that the aged and fresh graphite anodes have the same EC amount. Table 1 summarizes the peak intensity ratio of the typical organic (ROCOOLi, 1640 cm^{-1}) and inorganic (LiOH, 3680 cm^{-1}) species to EC (1770 cm^{-1}) obtained from Fig. 1(b). Obviously, the amount of ROCOOLi decreased with cycling, in contrast to the formation of LiOH on the graphite surface. This suggests that the amount of organic component decreased, in contrast to the increase of inorganic component.

3.2. XPS measurement

Next, we used XPS tool to study the nature and composition of surface layers formed on the graphite anode and $LiCoO_2$ cathode with or without cycling. While FTIR technique is only sensitive to certain types of functional-group vibrations, all characteristic elements can be detected by XPS analysis.

We first focused on the surface information of electrode layer with a thickness of a few nm. Figs. 2–5 show the C 1s, F 1s, O 1s, Li 1s and Co 3p, P 2p, and Co 2p core peak spectra of surface film for graphite anode and $LiCoO_2$ cathode obtained from fresh and aged lithium-ion cell. The corresponding results of quantitative analysis are reported in Table 2. Obviously, the atomic percentage of every element on electrode surface changed with cycling history and electrode type. Next, we investigated the depth profile information of surface films on graphite anode and $LiCoO_2$ cathode of the aged and fresh cells, as shown in Figs. 6 and 7.

3.2.1. C 1s spectra

Table 2 shows that the atomic percentage change of carbon occurred mainly on the graphite-anode surface, rather than the $LiCoO_2$-cathode surface. The atomic percentage of carbon on the graphite-anode surface decreased after prolonged cycling.

Table 3 summarizes the peak separating result for carbon based on the spectra of Figs. 2–5. The component of carbon

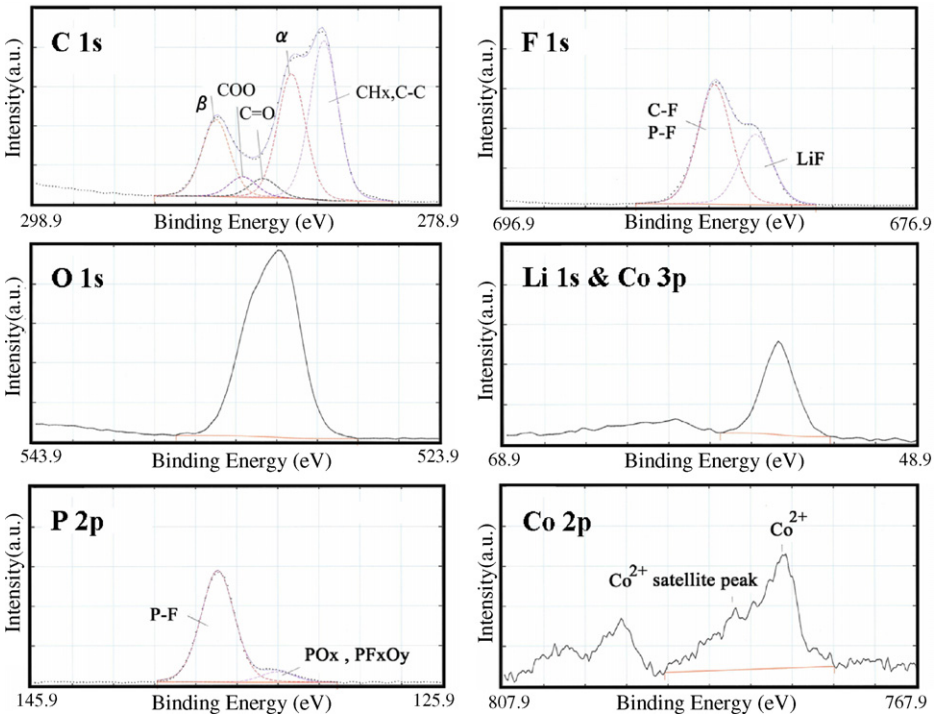

Fig. 2. XPS spectra of surface film for graphite anode obtained from fresh lithium-ion cell.

at the surface was similar in these samples. The C 1s spectra of samples show five main contributions. The CH_x, C–C and α components can be assigned to oligomers of polyethylene oxide (PEO, $(–CH_2–CH_2–O–)_n$), which was detected as the electrolyte degradation products of lithium-ion cells with cycling history [6]. The CH_x, C–C, C=O, COO and β components reveals the presence of Li_2CO_3 and ROCOOLi, which have been widely described as the main components of the surface layers forming on various electrodes exposed in EC-based electrolytes, and also identified by FTIR result in this work. There is somewhat difference in C=O, COO, and β components for both of electrodes. However, it is difficult to distinguish

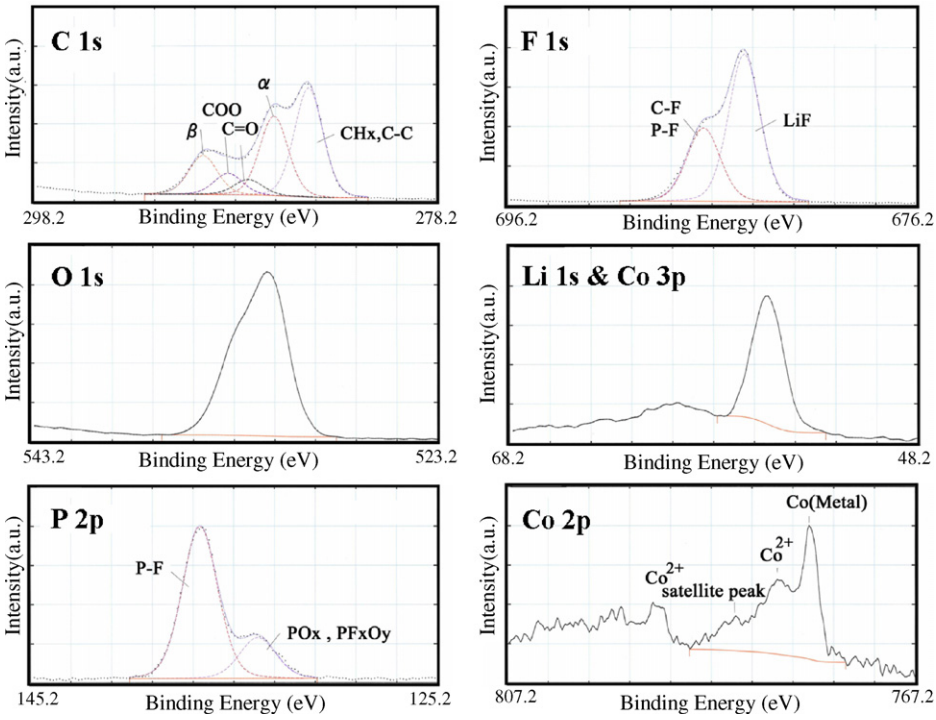

Fig. 3. XPS spectra of surface film for graphite anode obtained from aged lithium-ion cell.

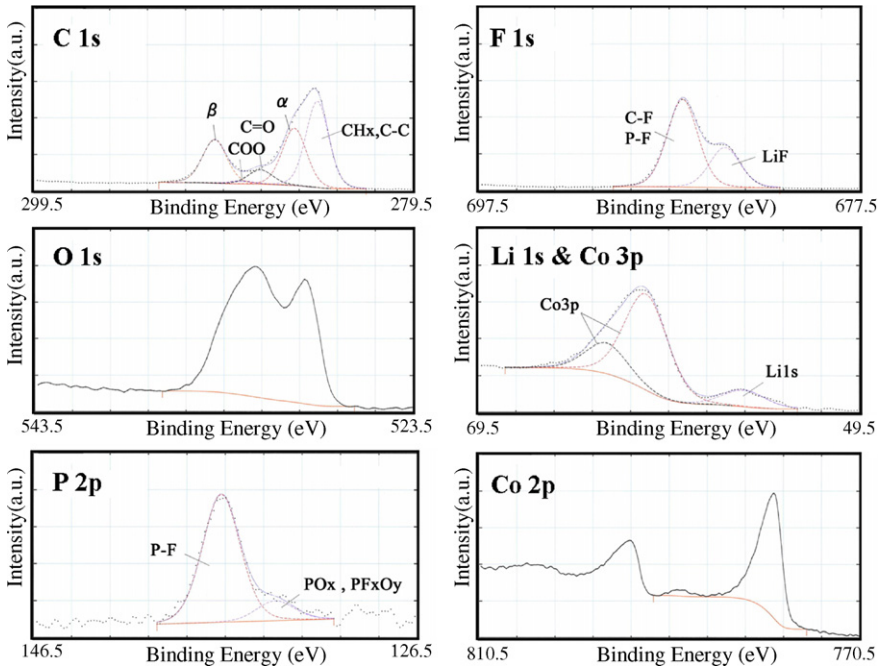

Fig. 4. XPS spectra of surface film for $LiCoO_2$ cathode obtained from fresh lithium-ion cell.

Li_2CO_3 and ROCOOLi based on the present data. In addition, poly(vinylidene fluoride) (PVdF) binder was identified by $-(CH_2-CF_2)_n-$ component, which has generally the same ratio at α component and β component.

3.2.2. F 1s spectra

The observed amounts of fluorine tended to increase due to charge–discharge cycling for the both electrodes (Table 2). This tendency was especially obvious for the graphite anode.

Table 4 summarizes the peak separating result for fluorine based on the spectra of Figs. 2–5. All spectra showed the first peak at 685.0 eV due to LiF, and the second at 687.2 eV due to the remaining $LiPF_6$ solute and PVdF binder. We believe that the formation of LiF at the interface unambiguously results from the decomposition of $LiPF_6$ solute, as described by other groups.

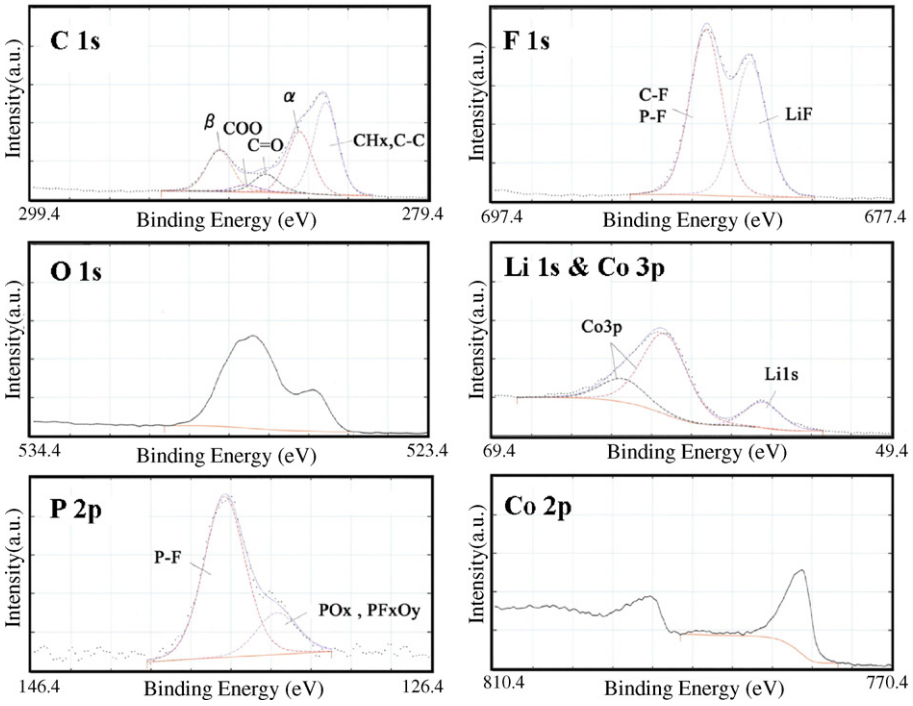

Fig. 5. XPS spectra of surface film for $LiCoO_2$ cathode obtained from aged lithium-ion cell.

Table 2
Atomic percentage of various elements on surface layer of graphite anode and $LiCoO_2$ cathode obtained from fresh and aged lithium-ion cells

Sample	Atomic percentage (%)					
	C	F	O	Li	P	Co
Anode						
Fresh	29.7	27.5	18.7	20.8	2.9	0.4
Aged	20.3	31.6	16.2	29.0	2.5	0.4
Cathode						
Fresh	41.1	28.1	15.2	12.4	0.9	2.3
Aged	39.3	29.2	15.4	13.4	1.2	1.5

Therefore, we can reasonably attribute the fluorine increase with cycling to LiF formation on the surface of both electrodes.

3.2.3. O 1s spectra

The observed amounts of oxygen at the surface was similar in the same electrode (15.2–15.4 at.% for cathode, and 16.2–18.7 at.% for anode). Since all oxygen-containing species present in the surface layer contribute to the observed spectrum, with very few variations of the binding energy, O 1s core peaks often provide very poor information. However, some points can be noticed in the XPS spectra of graphite-anode surface, as shown in Figs. 2 and 3. A maximum at 531.9 eV is the expected value for Li_2CO_3. The shoulder at around 533.5 eV may be

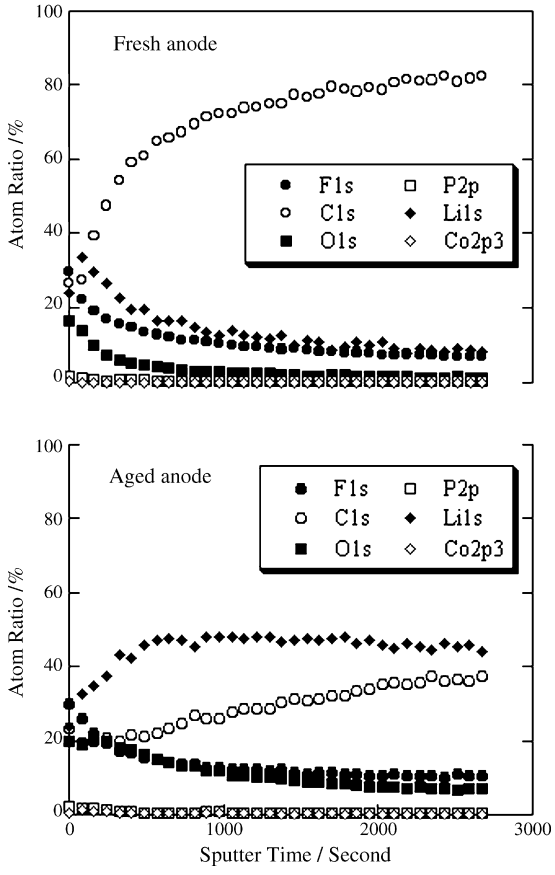

Fig. 6. Depth profiles of various species on graphite-anode surface of fresh and aged lithium-ion cells.

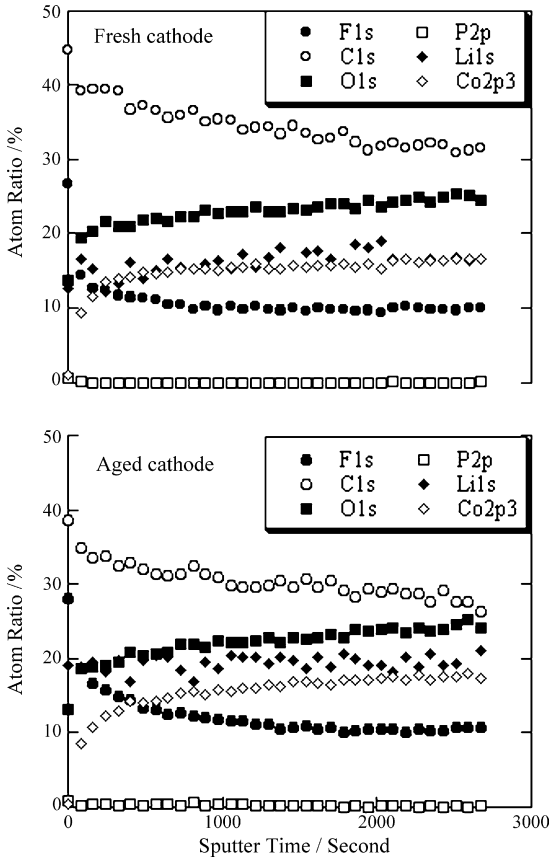

Fig. 7. Depth profiles of various species on $LiCoO_2$-cathode surface of fresh and aged lithium-ion cells.

Table 3
Separation result of C 1s peak as shown in Figs. 2–5

Sample	Component (%)				
	CH_x, C—C	α[a]	C=O	COO	β[b]
Anode					
Fresh	40	31	5	5	19
Aged	41	30	6	8	15
Cathode					
Fresh	41	29	7	1	22
Aged	41	29	8	3	19

[a] —(C^*H_2—CF_2)$_n$—, C—O.
[b] —(CH_2—C^*F_2)$_n$—, CO_3^{2-}, —OCOO—, —CF—.

Table 4
Separation result of F 1s peak as shown in Figs. 2–5

Sample	Component (%)	
	LiF	C—F, P—F
Anode		
Fresh	37	63
Aged	66	34
Cathode		
Fresh	31	69
Aged	45	55

Table 5
Separation result of P 2p peak as shown in Figs. 2–5

Sample	Component (%)	
	PO_x, PFO_x	P—F
Anode		
Fresh	9	91
Aged	22	78
Cathode		
Fresh	13	87
Aged	21	79

an expected shape for ROCOOLi. Thus, these observations are in good agreement with C 1s XPS spectra and FTIR results. Comparing Figs. 2 and 3 discloses that ROCOOLi component decreases with cycling, in contrast to Li_2CO_3 component.

3.2.4. Li 1s spectra

The lithium amount obviously increased at graphite-anode surface after prolonged cycling (Table 2). The variation of the binding energy is rather faint, between 55.6 and 55.8 eV, as shown in Figs. 2–7. Taking into account that Li_2CO_3 gives a Li 1s peak at 55.5 eV, LiF at 55.9 eV, and $LiPF_6$ at 57.2 eV, no real conclusion can be made on the relative amount of Li-containing species.

3.2.5. P 2p spectra

The signal-to-noise ratio of these spectra is rather low because the amount of phosphorus in the samples was only 1–3 at.%, as shown in Figs. 2–5. All spectra are very similar, showing a peak at 136.9 eV assigned to $LiPF_6$, and a shoulder at 134.0 eV assigned to decomposition products of $LiPF_6$. Several authors have proposed degradation products such as phosphate (PO_x, PFO_x) [21]. The peak separating result of phosphorus in Table 5 disclosed that the decomposition products of $LiPF_6$ increased due to cycling history.

3.2.6. Co 2p spectra

Different from the common XPS studies on surface chemistry, we paid an additional attention on the cobalt species. Figs. 2–5 present the Co 2p XPS spectra on the surface layer of graphite anode and $LiCoO_2$ cathode with and without cycling history. Co^{2+} ion was detected for both anodes, and Co^{3+} ion for both cathodes, independent of cycling history. It is worth noting that the Co metal existed on the aged graphite-anode surface. To our knowledge, this is a new finding for Co metal deposited at graphite-anode surface though Aurbach group reported Co species on the lithium electrode [31]. This may be attributed to the aged sample used in this work which experienced a long-term charge–discharge cycle. We believe that a part of Co^{2+} ion can be irreversibly converted to Co metal at graphite surface during charging.

3.2.7. Depth profile

Fig. 6 discloses a large difference in depth profile of surface species on aged and fresh graphite anodes. Overall, the contents of fluorine, oxygen, phosphorus and cobalt were high at surface layer of both graphite anodes, and decreased with sputtering duration. In particular, the aged graphite-anode surface had much more lithium and oxygen from surface layer through inner layer than that on the fresh graphite-anode surface. The fluorine, phosphorus and cobalt are also more at the aged graphite-anode surface than those at the fresh graphite-anode surface. These findings indicate that the surface film at the graphite-anode surface becomes thicker due to continuous growth of surface species as indicated above with cycle number and covers all the graphite particles.

The prolonged cycling gives small effect on depth profile of various species at surface layer of $LiCoO_2$ cathode, as shown in Fig. 7. Only slight increase in fluorine, lithium, and phosphorus contents was observed for the aged $LiCoO_2$ cathode.

3.3. Discussion

Table 6 summarizes the surface species detected by FTIR and XPS spectra. Though most of the surface species may be identified by two analysis approaches, the FTIR and XPS tend to be sensible to organic species and inorganic compounds, respectively. Especially, we detected Co metal at the aged graphite-anode surface which was produced during the long-term cycle-life testing. This is a very interesting finding since $LiCoO_2$ cathode is sole resource of Co species. Aurbach and

Table 6
Summary of surface species detected by FTIR and XPS spectra

Sample	Surface species	Note
Anode		
Fresh	ROCOOLi[a], Li_2CO_3[a], EC[b], $LiPF_6$[a], PEO[c], PVdF[c], LiF[c], phosphate[c], Co^{2+}[c]	Organic film: more
Aged	ROCOOLi[a], Li_2CO_3[a], LiOH[b], EC[b], $LiPF_6$[a], PEO[c], PVdF[c], LiF[c], phosphate[c], Co^{2+}[c], Co metal[c]	New species: LiOH, Co metal. Inorganic film: more
Cathode		
Fresh	ROCOOLi[a], Li_2CO_3[a], EC[b], $LiPF_6$[a], PEO[c], PVdF[c], LiF[c], phosphate[c], Co^{3+}[c]	Less change in amount and species than anode
Aged	ROCOOLi[a], Li_2CO_3[a], EC[b], $LiPF_6$[a], PEO[c], PVdF[c], LiF[c], phosphate[c], Co^{3+}[c]	

[a] Detected by both FTIR and XPS.
[b] Detected by FTIR only.
[c] Detected by XPS only.

co-workers have found Co dissolution from $LiCoO_2$ cathode during cycling and demonstrated a direct correlation among the degree of capacity fading, the amount of Co^{2+} ion in the electrolytes, and structure changes [31,32]. To a certain extent, the above demonstration is similar to the well-known Mn dissolution from $LiMn_2O_4$ electrode which results in the structure and chemical instability of the $LiMn_2O_4$ electrode, and hence causes the capacity loss following the mechanism described by Tarascon and co-workers [33]. We believe that there is dissolution equilibrium between Co^{2+} ion and $LiCoO_2$ cathode in a carbonate-based electrolyte. During prolonged cycling, the reduction reaction of Co^{2+} ion produces Co metal at graphite anode surface, which destroys the above dissolution equilibrium and increases Co^{2+} ion dissolution. The main detrimental effect of Co dissolution from $LiCoO_2$ cathode is the capacity loss through promoting the structure destruction of $LiCoO_2$. It is also possible that the Co metal at graphite anode surface causes micro-short when the amount of Co metal is enough to form a short circuit.

In a common concept, the surface film should become thick with cycling due to increasing electrolyte decomposition. This knowledge was indeed confirmed by depth profile of XPS analysis, where we found that the surface film at the aged graphite anode became thicker than that at the fresh graphite anode. We further estimated the amount of various species in surface films by FTIR analysis, as summarized in Table 1. We note that the amount of organic film at graphite surface decreased with cycling. In fact, this surface phenomenon was also reported in another paper, where the authors thought that there was either an increase in the inorganic component with cycling or a conversion from organic to inorganic components [34]. Since XPS analysis also disclosed that the amount of inorganic (organic) components increased (decreased) with cycling in this work, we can reasonably propose the following mechanism to explain the surface phenomena of anode and cathode experiencing prolonged cycling.

(i) SEI film consisting of primary organic components and a part of inorganic components is formed at the electrode surface after the electrode is immersed into the carbonate electrolyte. The organic components come from reduction (oxidation) decomposition of carbonate solvents, such as EC, for anode (cathode).
(ii) The above SEI formation stops once the film is thick enough to prevent electron tunneling.
(iii) During prolonged cycling, the redox reaction between organic components at electrode surface and inorganic species in the electrolyte becomes the main surface reaction. Consequently, the amount of inorganic (organic) components increases (decreases).

Generally, the inorganic components are known to have high impedance. The increase in inorganic components with cycling is also a cause of cell-performance degradation.

The results in papers I and II suggest that the prolonged cycling exhibited different impacts on cathode and anode. While the cathode had large structure destruction and small change in surface chemistry, the anode showed a slight structure destruction and severe change in surface chemistry. As concluded in paper I, the serious structure change in $LiCoO_2$ cathode is primarily responsible for the performance degradation of the aged lithium-ion cell experiencing long-term cycle-life testing. However, there is a correlation of cathode structure destruction with anode surface chemistry, as observed from Co metal at graphite surface. We believe that the Co metal deposited at graphite surface may promote the structure destruction of $LiCoO_2$ cathode, as described above.

4. Conclusions

We characterized the surface chemistry of $LiCoO_2$ cathode and graphite anode in an aged commercial laminated lithium-ion cell experiencing 4350-cycle charge–discharge in a simulated LEO satellite operation by FTIR and XPS analysis. This is a sequent work to investigate the performance-degradation mechanism of the aged cell experiencing the prolonged cycling.

Overall, the graphite anode had a larger change in surface chemistry than that of the $LiCoO_2$ cathode. Except the common components, such as ROCOOLi, LiOH, Li_2CO_3, and PEO, we detected Co metal at the aged graphite surface. It is the first time to report Co metal at the graphite anode surface as a result of prolonged cycling. We proposed a mechanism to explain this phenomenon, and deduced that Co metal deposition was detrimental to structure stability of $LiCoO_2$ cathode which was a main cause of cell capacity loss. We estimated the amount of various species in surface films by FTIR analysis. We found that the organic (inorganic) film decrease (increase) with prolonged cycling though the total amount of surface component increased. This has been attributed to the redox reaction between organic components at electrode surface and inorganic species in the electrolyte.

It may be concluded that the structure destruction of $LiCoO_2$ cathode was the primary cause of cell-performance degradation. Some surface chemistry at graphite anode, such as Co metal deposition, may promote the structure destruction of $LiCoO_2$ cathode and accelerate the cell-performance degradation.

Acknowledgments

The authors would like to acknowledge the technical staffs from Ryoei Technica Corporation for their support. *Japan Aerospace Exploration Agency (JAXA) assisted in meeting the publication costs of this article*.

References

[1] D. Aurbach, O. Chusid, J. Power Sources 68 (1997) 463.
[2] V. Eshkenazi, E. Peled, L. Burstein, D. Golodnitsky, Solid State Ionics 170 (2004) 83.
[3] E. Peled, D.B. Tow, A. Merson, A. Gladkich, L. Burstein, D. Golodnitsky, J. Power Sources 97–98 (2001) 52.
[4] M. Letellier, F. Chevallier, C. Clinard, E. Frackowiak, J.N. Rouzaud, F. Beguin, M. Morcrette, J.M. Tarascon, J. Chem. Phys. 118 (2003) 6038.
[5] M.C. Smart, B.V. Ratnakumar, S. Surampudi, Y. Wang, X. Zhang, S.G. Greenbaum, A. Hightower, C.C. Ahn, B. Fultz, J. Electrochem. Soc. 146 (1999) 3963.

[6] H. Ota, Y. Sakata, X.M. Wang, J. Sasahara, E. Yasukawa, J. Electrochem. Soc. 151 (2004) A437.
[7] G. Nazri, R.H. Muller, J. Electrochem. Soc. 132 (1985) 2050.
[8] D. Aurbach, A. Zaban, J. Electroanal. Chem. 367 (1994) 15.
[9] D. Aurbach, Y. Cohen, J. Electrochem. Soc. 143 (1996) 3525.
[10] D. Aurbach, Y. Cohen, J. Electrochem. Soc. 144 (1997) 3355.
[11] D. Aurbach, A. Zaban, O. Chusid, I. Weissman, Electrochim. Acta 39 (1994) 51.
[12] D. Aurbach, B. Markovsky, A. Shechter, Y. Ein-Eli, H. Cohen, J. Electrochem. Soc. 143 (1996) 3809.
[13] D. Aurbach, A. Zaban, A. Shechter, Y. Ein-Eli, E. Zinigrad, B. Markovsky, J. Electrochem. Soc. 142 (1995) 2873.
[14] R. Spotnitz, J. Power Sources 113 (2003) 72.
[15] M. Wohlfahrt-Mehrens, C. Vogler, J. Garche, J. Power Sources 127 (2004) 58.
[16] M. Broussely, S. Herreyre, P. Biensan, P. Kasztejna, K. Nechev, R.J. Staniewicz, J. Power Sources 97 (2001) 13.
[17] R. Yazami, Electrochim. Acta 45 (1999) 87.
[18] E. Peled, J. Electrochem. Soc. 126 (1979) 2047.
[19] E. Peled, in: J.-P. Gabano (Ed.), Lithium Batteries, Academic Press, New York, 1983, p. 43.
[20] J.R. Dahn, A.K. Sleigh, H. Shi, B.M. Way, W.J. Weydanz, J.N. Reimers, Q. Zhong, U. von Sacken, in: G. Pistoia (Ed.), Lithium Batteries: New Materials, Developments, and Perspectives, Elsevier, Amsterdam, 1994.
[21] R. Dedryvere, S. Laruelle, S. Grugeon, L. Gireaud, J.-M. Tarascon, D. Gonbeau, J. Electrochem. Soc. 152 (2005) A689.
[22] S. Grugeon, S. Laruelle, S. Dupont, J.-M. Tarascon, Solid State Sci. 5 (2003) 895.
[23] S. Zhang, K. Xu, T.R. Jow, J. Electrochem. Soc. 149 (2002) A1521.
[24] D. Aurbach, M.D. Levi, E. Levi, H. Teller, B. Markovsky, G. Salitra, U. Heider, L. Heider, J. Electrochem. Soc. 145 (1998) 3024.
[25] Y. Matsuo, R. Kostecki, F. McLarnon, J. Electrochem. Soc. 148 (2001) A687.
[26] J.K. McDermott, in: J.R. Wertz, W.J. Larson (Eds.), Space Mission Analysis and Design, third ed., The Space Technology Library, California, 1999, p. 407.
[27] Y. Sone, X. Wang, H. Kusawake, S. Kuwajima, Proceedings of the 2002 NASA Aerospace Battery Workshop (CD-ROM Version), Marshall Space Flight Center, Huntsville, USA, 2003.
[28] X. Wang, Y. Sakiyama, Y. Takahashi, C. Yamada, H. Naito, G. Segami, T. Hironaka, E. Hayashi, K. Kibe, J. Power Sources 167 (2007) 162.
[29] D. Aurbach, A. Zaban, J. Electroanal. Chem. 348 (1993) 155.
[30] D. Aurbach, B. Markovsky, M.D. Levi, A. Schechter, M. Moshkovich, Y. Cohen, J. Power Sources 81–82 (1999) 95.
[31] B. Markovsky, A. Rodkin, G. Salitra, Y. Talyosef, D. Aurbach, H.-J. Kim, J. Electrochem. Soc. 151 (2004) A1068.
[32] D. Aurbach, B. Markovsky, A. Rodkin, E. Levi, Y.S. Cohen, H.-J. Kim, M. Schmidt, Electrochim. Acta 47 (2002) 4291.
[33] G. Amatucci, A.D. Pasquier, A. Blyr, T. Zheng, J.-M. Tarascon, Electrochim. Acta 45 (1999) 255.
[34] M. Herstedt, D.P. Abraham, J.B. Kerr, K. Edstrom, Electrochim. Acta 49 (2004) 5097.